Heliyon 9 (2023) e18350

Contents lists available at ScienceDirect

Heliyon

journal homepage: www.cell.com/heliyon

Conversion and rate behavior of brown macroalgae in pyrolysis: Detailed effects of operating parameters

Apip Amrullah [a,b,*], Obie Farobie [c,d]

[a] Department of Mechanical Engineering, Lambung Mangkurat University, Banjarmasin, South Kalimantan, Indonesia
[b] Division for Biomass and Energy, Wetland-Based Material (WBM) Research Center, Lambung Mangkurat University, Banjarmasin, South Kalimantan, Indonesia
[c] Department of Mechanical and Biosystem Engineering, Faculty of Agricultural Engineering and Technology, IPB University (Bogor Agricultural University), IPB Darmaga Campus, PO BOX 220, Bogor, West Java 16680, Indonesia
[d] Surfactant and Bioenergy Research Center (SBRC), IPB University (Bogor Agricultural University), Jl. Pajajaran No. 1, IPB Baranangsiang Campus, Bogor, West Java 16144, Indonesia

ARTICLE INFO

Keywords:
brown macroalgae
Operating parameter
Pyrolysis
Tar formation
Rate constant

ABSTRACT

Non-catalytic pyrolysis of brown macroalgae (Padina sp.) was studied in a batch reactor at temperature ranges of 400–600 °C and 10–90 min reaction times on the product distribution and conversion rate behavior. The highest pyro-oil and pyro-gas yields were obtained at 600 °C, which reached 67 wt% and 27 wt%, respectively, when the reaction times were prolonged (30–90 min). In addition, the high reaction temperature resulted in more generations of heavy tar and a considerable enhancement in aromatization degree. N-aromatic groups and phenol were observed from pyro-oil at 500 °C and 600 °C, respectively. Tar yield increased with reaction temperature, reflecting an order of reaction greater than one for tar production. The rate constant of tar formation was found to be 0.0013/s at 400 °C; 0.0023/s at 500 °C; and 0.0033/s at 600 °C, respectively, with the reaction order being higher than one (1.25). These findings highlighted that the proposed model could be used to accurately predict the pyrolysis process's behavior.

1. Introduction

The reliance on fossil fuels alone is problematic on multiple fronts, including the economy and the environment. A great energy crisis has directly resulted from the unstable international political scenario [1]. Consequently, there is widespread support around the globe for replacing fossil fuels with sustainable energy sources like biomass. In addition, many governments have set the goal of reaching Net Zero Emissions by 2050, and renewable energy has been considered a vital part of that effort [2]. This is because biomass is regarded as carbon neutral, unlike fossil fuels. The utilization of lignocellulosic biomass still needs to improve with competition for land and freshwater use, besides the need for fertilizers [3,4]. However, as an alternative to terrestrial biomass, macroalgae are an appealing option considering that they are aquatic species that can thrive in the ocean, have a rapid growth rate, do not require arable land, and have a significant organic matter content [5].

Indonesia, which boasts one of the world's longest coastlines and largest ocean areas, is home to various unusual marine species [6]. Seaweed, or macroalgae, is one example. For generations, maritime societies have relied on seaweed for food and medicine.

* Corresponding author. Jl. Brigjen H. Hasan Basri, Kayu Tangi, Banjarmasin, Kotak Pos 219, Indonesia.
E-mail address: apip.amrullah@ulm.ac.id (A. Amrullah).

https://doi.org/10.1016/j.heliyon.2023.e18350
Received 5 April 2023; Received in revised form 6 July 2023; Accepted 13 July 2023
Available online 17 July 2023

Production in 2019 is expected to reach 9.9 million tons, making Indonesia the world's second-largest seaweed producer behind China [7]. However, *Gracillaria* sp., *Gelidium* sp., and *Euchema* sp. are the most often used species in industrial applications. Moreover, most of Indonesia's seaweed exports are raw materials with limited added value. In contrast, only a percentage of the total is exported in a processed form, offering incredible economic benefits in sectors like the food and pharmaceutical industries [8]. Considering the massive potential of seaweed, Indonesia is being challenged to improve its use and added value by diversifying its product for use in various industries, including food, feed, fertilizer, pharmaceuticals, and cosmetics [9].

In the meantime, Indonesia is working toward its goal of reaching Net Zero Emissions by the year 2060. Increasing the proportion of renewable energy derived from biomass in the country's overall energy mix is one initiative [10]. Because of its organic content, macroalgae can be turned into bio-oil and solid fuel for energy sources; however, this application path must be included. After being improved, bio-oil can replace fossil fuels in many ways, such as a fuel to make heat, electricity, and chemicals. Bio-oil with better quality can be used in boilers, furnaces, turbines, diesel engines, power plants, and other industrial processes [11,12]. As to produce chemicals, bio-oil can be further treated to get phenol for resins and wood adhesives, molded plastic, and foam insulation. Research has shown that macroalgae could be the source of bio-oil and hydrochar via the thermochemical process. Thermochemical processes are considerably faster than biochemical processes and are frequently employed to enhance biofuel generation from biomass [13]. Among the thermochemical conversion techniques for biomass, the pyrolysis process is most designed to produce biofuels [14,15]. Pyrolysis is one-way that biomass can be changed thermochemically to produce energy and chemicals. Without oxygen, biomass can be used to produce gas, oil, and char [16].

Several studies have reported bio-oil production potential from macroalgae. Verma et al. (2021) [17] investigated a different study that examined the catalytic and reaction parameters of the pyrolysis of Ulva lactuca macroalgae on bio-oil production. They concluded that a bimetallic Co–Ni/ZrO2 catalyst produced the most bio-oil (49.2 wt%), showing that both metals work together to break down biomass and improve bio-oil. Ly et al. (2015) [18] examined the effects of varying temperatures, flow rates, and feedstock particle sizes on the pyrolysis of *Saccharina japonica*. The maximum bio-oil obtained in their study was 44.99% at 350 °C. Furthermore, Farobie et al., (2022a) [19] investigated the bio-oil and biochar production from *Sargassum* sp. via slow pyrolysis. They found that significant compounds could be identified in bio-oil from *Sargassum* sp., including carboxylic acids, furan derivatives, aliphatic hydrocarbons, and N-aromatic compounds.

Previous studies give insights that bio-crude oil and biochar can be produced from macroalgae via pyrolysis. However, until now, no previous study has reported a detailed study on the pyrolysis of brown macroalgae *Padina* sp. in terms of the effect of operating parameters and kinetic study. *Padina* sp. is selected since it is one of the species of macroalgae mostly found in Indonesia [20]. Therefore, the key objectives of this study are (1) to elucidate the effect of pyrolysis parameters on the product distribution and bio-oil characteristics during the pyrolysis of *Padina* sp. and (2) to evaluate the kinetic behavior of brown algae *Padina* sp. degradation during pyrolysis.

2. Materials and methods

2.1. Material

The macroalgae of the *Padina* sp. species used in this study were obtained from Lombok, located in the western part of Nusa Tenggara. Initially, the feedstock was washed with normal water to remove sand or debris. After that, the cleaned feedstock was dried in an oven (105 °C for 24 h) before being placed on a grinder fitted with a sieve and reduced to a constant particle size of 0.3 mm. A thermogravimetric analyzer (TGA 4000; PerkinElmer, USA) was used to determine feedstock proxies following ASTM E1131-08. The proximtae analysis showed a high volatile matter concentration in *Padina* sp. (51.92%). Therefore, biomass with a high volatile matter content may be useful as an energy source. *Padina* sp. has moisture (11.29%), fixed carbon (9.01%), and ash (28.50%) content.

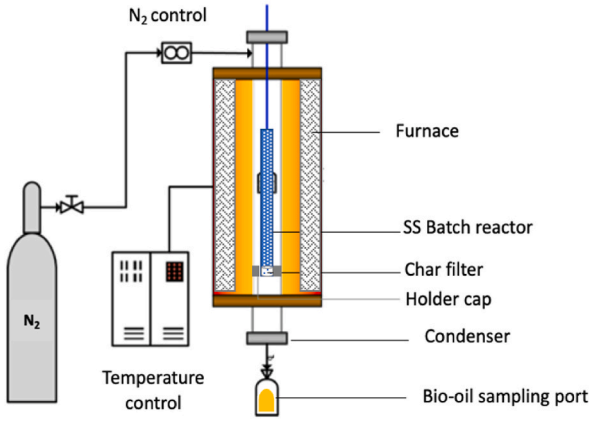

Fig. 1. Schematic diagram of experimental apparatus.

2.2. Batch pyrolysis experiments

The pyrolysis was carried out in a stainless-steel batch reactor (Fig. 1). The reactor had a condenser, an electric burner, and a thermocouple. The highest temperature at which the reactor can operate is 1000 °C. A PID temperature controller is used to control the temperature. Briefly, 50 g of dried *Padina* sp. was added to the reactor as feedstock. A 100 mL min^{-1} flow of nitrogen gas was used for flushing the reactor to eliminate any traces of oxygen.

After confirming that the atmosphere was at the standard temperature, the reactor was gradually heated to 400, 500, and 600 °C at 30 °C per minute. During the pyrolysis process, the products in the vapor phase were allowed to condense and collected through a liquid sample port. After the reactor had cooled down, the biochar was removed, and its weight was measured digitally. Tar was collected by absorbing the liquid products and washing the entire cooling pipeline with isopropanol (tar protocol [21]), with the water content separated using a separating funnel (the water-soluble organic materials were neglected in all runs). Every single test was done three times. The yield of products was calculated using the following formula (1)-(4):

$$Y_{tar} = \frac{m_{tar+pyrooil} - C_{slt} \times m_{pyrooil}}{m_{feedstock\ [dry]}}\ 100\% \tag{1}$$

$$Y_{pyro-oil} = \frac{m_{pyrooil}}{m_{feedstock\ [dry]}} \times 100\% \tag{2}$$

$$Y_{solid} = \frac{m_{solid}}{m_{feedstock\ [dry]}} \times 100\% \tag{3}$$

$$Y_{pyro-gas} = \left(1 - Y_{tar} + Y_{pyrooil} + Y_{solid}\right) \times 100\% \tag{4}$$

where $m_{tar+pyrooil}$ is the mass of pyro-oil product [g]; C_{slt} is the water content of solution [g]; $m_{pyrooil}$ is the initial mass content of the pyro-oil product [g]; and m_{solid} and $m_{feedstock}$ are the mass content of solid product and feedstock (dry basis), respectively [g].

2.3. Product analyses

Pyro-oil samples were analyzed using a GC–MS (QP-2010) with a capillary column coated with white Rtx-5MS (i.d. 60 mm × 0.25 mm and film thickness of 0.25 μm). 1 mL of the sample was mixed with methanol and injected into the column. The GC temperature program started at 150 °C and stayed at that temperature for 5 min. The temperature then went up to 300 °C. Using the standard solution, each compound was identified. Due to laboratory limitations, the water-soluble compounds were not determined and analyzed for composition. After the experiment, the solid product was taken and dried overnight in a desiccator. It was then weighed until the weight was comparable. The final analysis used a CHNOS analyzer (VarioEL III, Germany). Using the VarioEL III, Germany CHNSO analyzer, the common organic elements such as C, H, N, S, and O were examined. The sample (1 mg) was placed in a tin boat to analyze the percentage composition of C, H, N, and S, and the percentage of O was measured by difference. In the case of pyro-gaseous, it is essential to point out that due to defective equipment, pyro-gas were not collected and examined for this particular study.

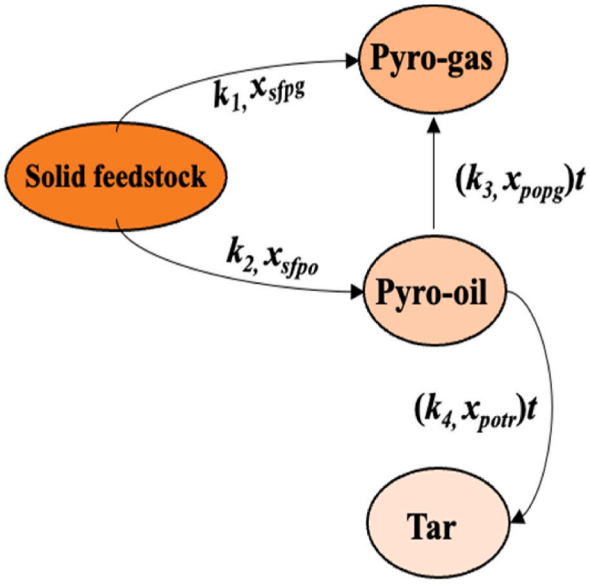

Fig. 2. Reaction pathways employed for analysis of the kinetics of macroalgae conversion.

Alternatively, the yield (%) of the other products is determined.

2.4. Reaction model

After obtaining data that revealed the impact of the operating parameters on macrolagae decomposition in the presence of pyrolysis, the following step was to apply a kinetic model to the data to glean information that helped understand the reaction kinetics of macroalgae decomposition. This was accomplished by fitting the data to the model. An investigation of the kinetics of the degradation of macroalgae was carried out using the reaction pathways illustrated in Fig. 2.

As will be seen below, there are four possible reactions to be considered appropriately:

$$(solid\ feedstock) \rightarrow (pyro-gas) \tag{5}$$

$$(solid\ feedstock) \rightarrow (pyro-oil) \tag{6}$$

$$(pyro-oil) \rightarrow (pyro-gas) \tag{7}$$

$$(pyro-oil) \rightarrow (tar) \tag{8}$$

k and *x* represent reaction rate constants and reaction orders, respectively, and Eqs (5)–(8) are expressed by sfpg, sfpo, popg, and potr, respectively. Eqs should express the reaction equation. (9) – (15) using concentration.

$$-\left[\frac{dC\ (feedstock)}{dt}\right]_k = \left[\frac{dC\ (pyro-oil)}{dt}\right]_{k_2} = \left[\frac{dC\ (pyro-gas)}{dt}\right]_{k_1} = k_{1,2}\ C(feedstock) \tag{9}$$

$$-\left[\frac{dC\ (pyro-oil)}{dt}\right]_{k_3 t} = \frac{1}{6}\left[\frac{dC\ (pyro-gas)}{dt}\right]_{k_3 t} = k_3 t\ C(pyro-oil) \tag{10}$$

$$-\left[\frac{dC\ (pyro-oil)}{dt}\right]_{k_4 t} = \left[\frac{dC\ (tar)}{dt}\right]_{k_4 t} = k_4 \mathrm{t}\ C(pyro-oil)^{X_{potr}t} \tag{11}$$

Then, the following equations are obtained.

$$\frac{dC\ (feedstock)}{dt} = \left[\frac{dC\ (feedstock)}{dt}\right]_{k_1} = -k_1 C\ (feedstock) \tag{12}$$

$$\frac{dC\ (pyro-oil)}{dt} = \left[\frac{dC\ (pyro-oil)}{dt}\right]_{k_1} + \left[\frac{dC\ (pyro-oil)}{dt}\right]_{k_3 t} + \left[\frac{dC\ (pyro-oil)}{dt}\right]_{k_4 t}$$

$$= k_2 C\ (feedstock) - k_3 t\ C\ (pyro-oil) - k_4 t\ C\ (pyro-oil)^{X_{potr}t} \tag{13}$$

$$\frac{dC(pyro-gas)}{dt} = \left[\frac{dC(pyro-gas)}{dt}\right]_{k_1} + \left[\frac{dC(pyro-gas)}{dt}\right]_{k_3 t}$$

$$= k_1 C\ (feedstock) + 6k_3 t\ C\ (pyro-oil) \tag{14}$$

$$\frac{dC\ (tar)}{dt} = \left[\frac{dC\ (feedstock)}{dt}\right]_{k_1} = k_4 t\ C\ (pyro-oil)^{X^{potr}t} \tag{15}$$

where *C* (*feedstock*) = macroalga concentration [g], *C* (pyro-oil) = concentration of pyro-oil product [g], [pyro-gas] = concentration of gas product [g], *C* (tar) = concentration of tar production [g], and *t* = reaction time [min]. The rate constants were then generated using nonlinear least-squares regression to fit the model to the experimental data, and the correlation on the rate constant was determined by the Arrhenius equation (Eq. 16). Microsoft Excel's Solver add-in feature was utilized with a trial-and-error approach.

$$k = Ae^{\left(\frac{-Ea}{RT}\right)} \tag{16}$$

where T is the temperature of the reaction [K], *Ea* is the activation energy [kJ/mol], R is the reaction rate constant for a universal gas [8.314 J mol^{-1} K^{-1}, and A is the pre-exponential factor [s].

3. Results and discussion

3.1. Element analysis of feedstock and solid product

The calorific value and ultimate analysis of *Padina* sp. solid produced at 400 °C, 500 °C, and 600 °C are shown in Fig. 3.

The solid product formed from the pyrolysis of *Padina* sp. contained a high concentration of carbon, ranging from 47.45 to 50.78%, low hydrogen content, varying from 4.44 to 4.67%, and medium oxygen content, ranging from 40.10 to 41.31%. As shown in Fig. 3, the solid product had a carbon content higher than that of the macroalgal feedstock. In addition, the amount of carbon present in the solid product increased as the temperature increased. In the meantime, the O and H concentrations of the solid product were lower than those of the feedstock. This may be due to dehydration, decarboxylation, and decarbonylation reactions during pyrolysis. In contrast, the hydrogen content of the solid product reduced substantially with increasing temperature, with the trend being as follows: 4.67% (400 °C), 4.44% (500 °C), 4.31% (600 °C). In addition, there was a decreasing trend tendency for the oxygen concentration of the solid product as the temperature increased.

The aromatization and production of hydrogen gas (H_2) due to the generation of low molecular-weight hydrocarbons (CH_4, C_2H_6, or C_2H_4) was another possible cause for the low hydrogen content of the solid product. It should be noticed that as pyrolysis temperatures were raised, the nitrogen content of the solid product obtained from macroalgal pyrolysis decreased. This could be because nitrogen is released into the gas phase as the pyrolysis temperature increases. Interestingly, the HHV of solid product from the pyrolysis of macroalgae was between 20.96 and 22.25 MJ kg^{-1}, which is higher than that of low-ranked coals (12–25 MJ kg^{-1}) [22].

3.2. Product distribution

The pyrolysis products of the macroalgal feedstock were investigated at temperatures of 400 and 600 °C, with a temperature interval of 100 °C. Fig. 4 depicts the distribution of solid, pyro-oil, pyro-gas, and tar products at different pyrolysis temperatures.

Generally, with increasing pyrolysis temperature and reaction time, pyro-oil, pyro-gas, and tar increased while solid decreased. The highest pyro-oil yield and pyro-gas yield were obtained at 600 °C, which reached 67 wt% and 27 wt%, respectively, when the reaction times were prolonged (30–90 min). The pyro-oil yield obtained from this study is comparable with the previous study using an in-situ catalytic process. Agnihotri and Mondal, (2023) [23] mentioned that the maximum bio-oil yield 0f 56 wt% was achieved for in-situ catalytic of *Melia azedarach* sawdust at 550 °C within 60 min. It was not surprising that higher temperatures were preferred for gas production. In addition, the solid yields decreased significantly as the reaction time increased, indicating the apparent degradation of the algal biomass due to the cracking of heavy hydrocarbons. This finding aligns with the previous study of Choi et al. (2016) [24], who identified that holding *Saccharina japonica* longer during the pyrolysis process enhanced the bio-oil yield but reduced the biochar yield. The tar yield showed an overall increasing trend with an increase in pyrolysis temperature. The highest tar yield reached 16 wt% at 600 °C. Generally, as the temperature increases, the primary reactions take place to biomass decompose and generate tar compounds. Pyrolysis oil or pyro-oil comprises primary tars, with some secondary tars, as assumed in this study [25]. For instance, N-aromatic groups and phenol were observed from pyro-oil at 500 °C and 600 °C, respectively. It was found that the primary tars that were produced from low-temperature pyrolysis might go through two main reaction pathways. First, some of the primary tars condensed and underwent polymerization reactions, leading to heavy tars' production. Secondly, some of the primary tars were decomposed into minor molecular gases, which resulted in a significant reduction of tar as well as an increase in the production of permanent gases. Considering the mass balance, it is possible to verify the output yield of Padina. sp. after the pyrolysis process. New equipment and technology development relies heavily on mass balance calculations, particularly those involving the design of the material used and the sizing of the structure, dependent on factors such as temperature. Secondary products that can be integrated into the system must also be quantified to increase their overall value [26].

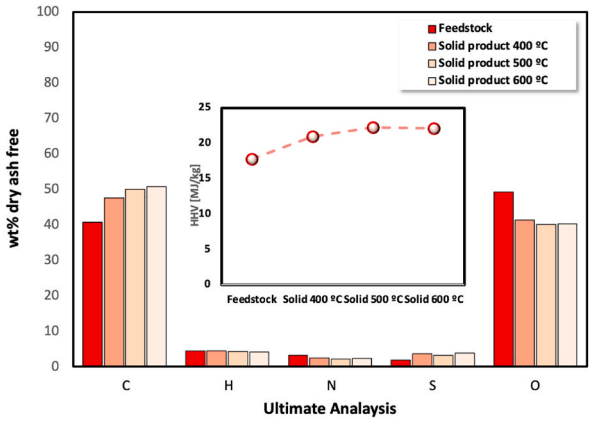

Fig. 3. Ultimate analysis of feedstock and solid product at 400, 500, and 600 °C.

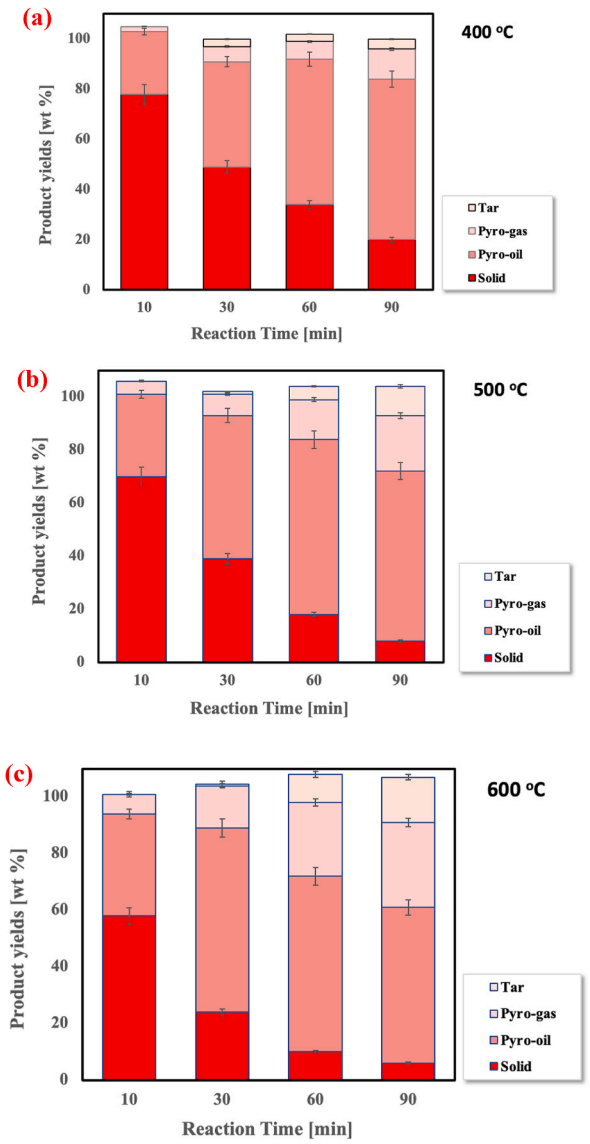

Fig. 4. Product yield at different pyrolysis temperatures (a) 400, (b) 500, and (c) 600 °C.

3.3. Pyor-oil production

Fig. 5 shows the chemical composition obtained from the pyrolysis of *Padina* sp. with the different pyrolysis temperatures. The bio-oil obtained from the pyrolysis of *Padina* sp. contained various chemicals.

It is worth mentioning that the bio-oil made from slow pyrolysis of *Padina* sp. was mostly carboxylic acid, N-aromatics, aliphatic hydrocarbons, phenol, ketones, alkanes, and amines/amides. For comparison, the peak area percentage of some compounds was used to determine how it changed with the pyrolysis temperature. At 400 °C, the percentage areas represented by compounds belonging to the carboxylic acid (carbon dioxide: 11.70%) and alkanes (Tetradecamethylheptasiloxane: 19.95%, Dodecamethylhexasiloxane: 12.0%, and Octadecamethylcycolonasiloxane: 11.2%), respectively, were found to be a major part of pyro-oil. It's worth noting that after pyrolyzing *Padina* sp. at 400 °C, small amounts of ketones and N-aromatic groups were also detected.

N-aromatic compounds are often generated via high-temperature pyrolysis of proteins, which results in their amino acids, which are then cyclized and aromatized to form N-aromatic compounds. The main component of N-aromatic compounds observed in this study was heterocyclic derivatives, such as 7-Hydroxy-7-phenyl-3,9-diisopropyl-2,10-dioxadispiro, pyrazine, 2,4 Imidazolidinedion, Morpholine, 4-Octadecyl, 3,5-Diphenyl-1-p. This study's results agree with those of a recent study by Iaccarino et al. (2021), which found that during the pyrolysis of *Salicornia bigelovii*, amino acids might undergo decarboxylation, cyclization, and dehydration to form the N-heterocyclic derivatives. Aliphatic hydrocarbons, which may be produced by the degradation of long-chain organic acids followed by a decarboxylation process, were also detected in the pyro-oil of *Padina* sp. In addition, a small amount of methane (8.32%)

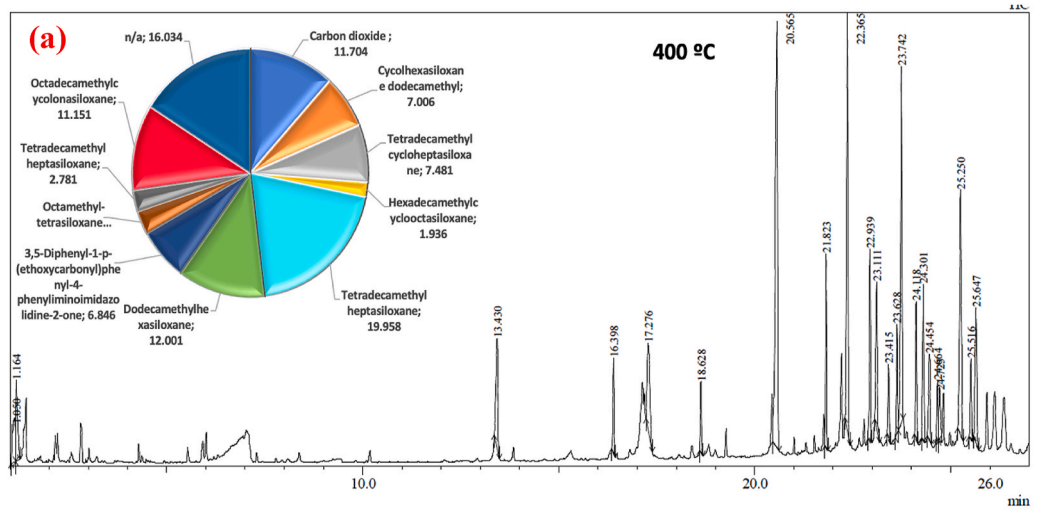

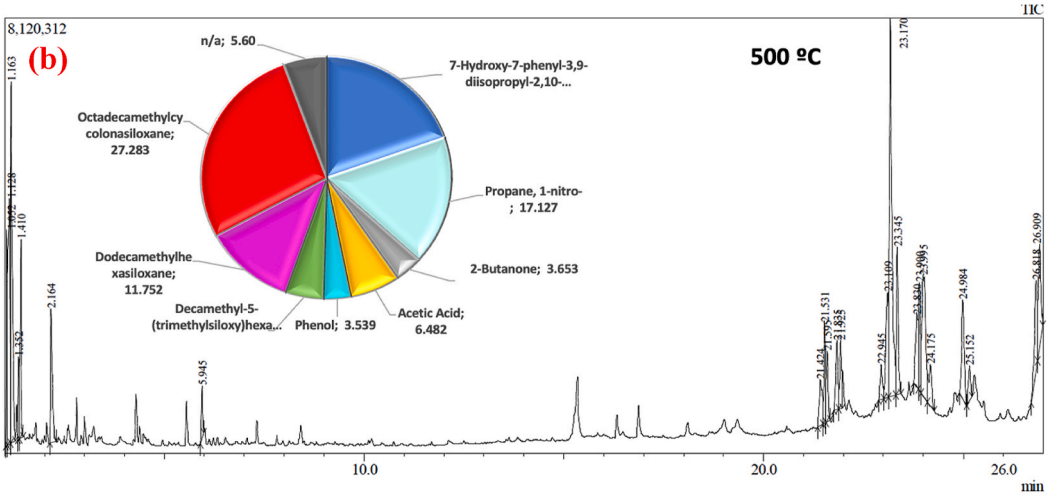

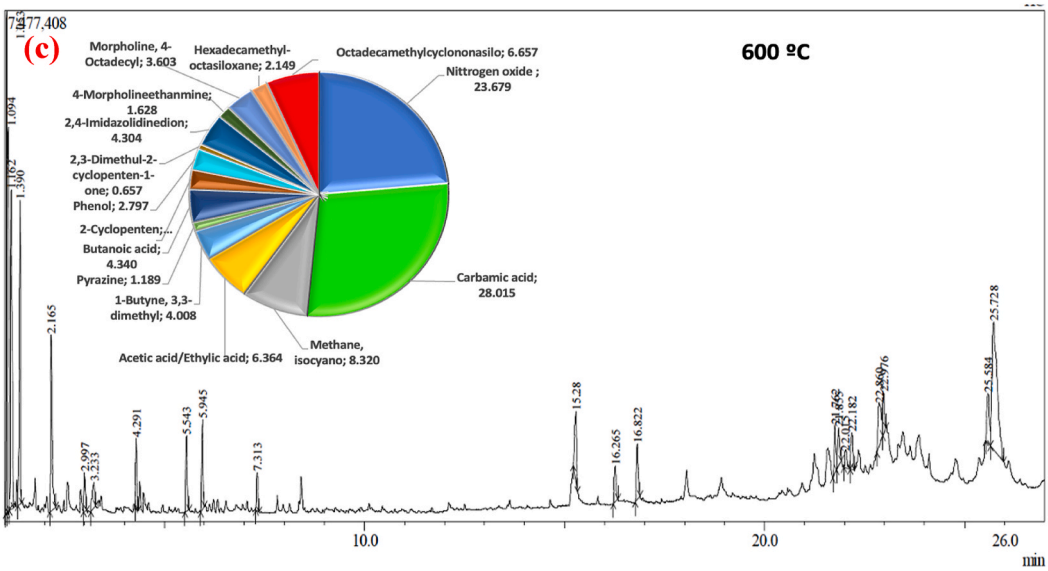

(caption on next page)

Fig. 5. GC/MS chromatogram of *Padina* sp. pyro-oil obtained at (a) 400 °C, (b) 500 °C, and (c) 600 °C.

was obtained from the pyrolysis of *Padina* sp. Finally, pyrolysis products of cellulose and hemicellulose degradation, including trace amounts of ketone derivatives (i.e., 7.06%), were detected.

In addition, the alkanes and amines groups decreased with increasing temperature for both 500 and 600 °C. Conversely, the ketones and N-aromatic groups were observed to behave in an opposite trend. Additionally, pyrolysis of *Padina* sp. generated phenolic compounds. As previously discussed, phenolic compounds might emerge from the steam reaction of aromatic compounds. Furthermore, the degradation of lignin or phenylalanine-containing protein has been attributed to producing phenolic compounds [27]. In this research, it was shown that the selectivity of phenolic compounds in pyro-oil decreased with increasing temperature, as follows: 3.54% (500 °C) > 2.7% (600 °C). This could be linked to higher temperatures promoting the disintegration of the main chain in phenolic compounds to produce hydrocarbons [28]. The summary of the general compounds by GC/MS is listed in Table 1.

3.4. Tar production

Fig. 6 shows that more tar is made when the pyrolysis temperature is raised. Tar is made of heavy molecules, and the order of reactions that lead to heavy molecules is higher than one. Thus, an increase in tar yield with increased pyrolysis temperature is attributed to the reaction order being greater than one for tar production (Eq. (8)), and the assumption of the first order for solid feedstock decomposition (Eq. (5) and Eq. (6)), and pyro-oil conversion (Eq. (7)) should be reasonable.

3.5. Kinetic parameters

Table 2 provides the kinetic parameters for the disappearance of macroalgae derived through the data-fitting approach. Meanwhile, Fig. 7 depicts the difference between the calculated (lines) and experimental product yields. The calculated results were very close to the experimental data.

It is worth noting that the reduction in the solid yield with an increasing temperature and prolonged reaction time is due to the production of pyro-gas, pyro-oil, and tar products. It should be noted that when all the reactions are first order, a common effect of product distribution is observed. In this case, the assumption of the first order for macroalgae degradation (Eq. (5)) and pyro-oil conversion (Eq. (7)) should be plausible. In contrast, the assumption of a higher reaction order for tar generation (Eq. (8)) is responsible for the elevation in pyrolysis temperature. The sequence of reactions leading to tar was determined to be 1.25. Activation

Table 1
Compounds identified in *Padina*'s sp. bio-oil at different experimental temperatures by GC/MS.

Residence time	Name	Molecular formula	Contentn (% Area)		
			400 °C	500 °C	600 °C
N-aromatic compounds					
1.052	7-Hydroxy-7-phenyl-3,9-diisopropyl-2,10-dioxadispiro	$C_{22}H_{28}O_5$	n.a	19.620	n.a
2.997	Pyrazine	$C_5H_6N_2$	n.a	n.a	1.189
15.283	2,4-Imidazolidinedion	$C_4H_6N_2O$	n.a	n.a	4.304
16.265	4-Morpholineethanmine	$C_6H_{14}N_2O$	n.a	n.a	1.628
16.821	Morpholine, 4-Octadecyl	$C_{22}H_{45}NO$	n.a	n.a	3.603
23.112	3,5-Diphenyl-1-p-(ethoxycarbonyl)phenyl-4-phenyliminoimidazolidine-2-one	$C_{30}H_{25}N_3O_3$	n.a	n.a	n.a
Carboxylic acids					
1.094	Carbamic acid	CH_3NO_2	n.a	n.a	28.015
1.128	Carbon dioxide	CO_2	11.704	n.a	n.a
1.39	Acetic acid/Ethylic acid	$C_2H_4O_2$	n.a	6.482	6.364
3.241	Butanoic acid	C_5H_{10} O_2	n.a	n.a	4.340
Aliphatic hydrocarbons					
1.16	Methane, isocyano	C_2H_3N	n.a	n.a	8.32
Ketone					
1.352	2-Butanone	C_4H_8O	n.a	3.653	n.a
2.16	1-Butyne, 3,3-dimethyl	C_6H_{10}	n.a	n.a	4.008
4.29	2-Cyclopenten	C_6H_8O	n.a	n.a	2.628
7.313	2,3-Dimethul-2-cyclopenten-1-one	$C_7H_{10}O$	n.a	n.a	0.657
13.428	Cycolhexasiloxane dodecamethyl	$C_{12}H_{36}O_6Si_6$	7.066	n.a	n.a
Phenol					
5.944	Phenol	C_6H_6O	n.a	3.539	2.71
Alkanes					
16.041	Tetradecamethylcycloheptasiloxane	$C_{14}H_{42}O_7Si$	2.781	n.a	n.a
21.427	Decamethyl-5-(trimethylsiloxy)hexasiloxane	$C_{13}H_{42}O_6Si_7$	n.a	4.944	n.a
21.763	Hexadecamethyl-octasiloxane	$C_{16}H_{50}$ O_7Si_8	10.205	n.a	2.149
22.184	Dodecamethylhexasiloxane	$C_{12}H_{38}$ O_5Si_6	12.001	11.752	0.611
Amines/Amides					
22.865	Eicosamethylcyclodecasiloxane	$C_{20}H_{60}O_{10}Si_{10}$	n.a	n.a	2.956
22.97	Octadecamethylcyclononasilo	$C_{18}H_{54}O_9Si_9$	11.151	27.283	6.657

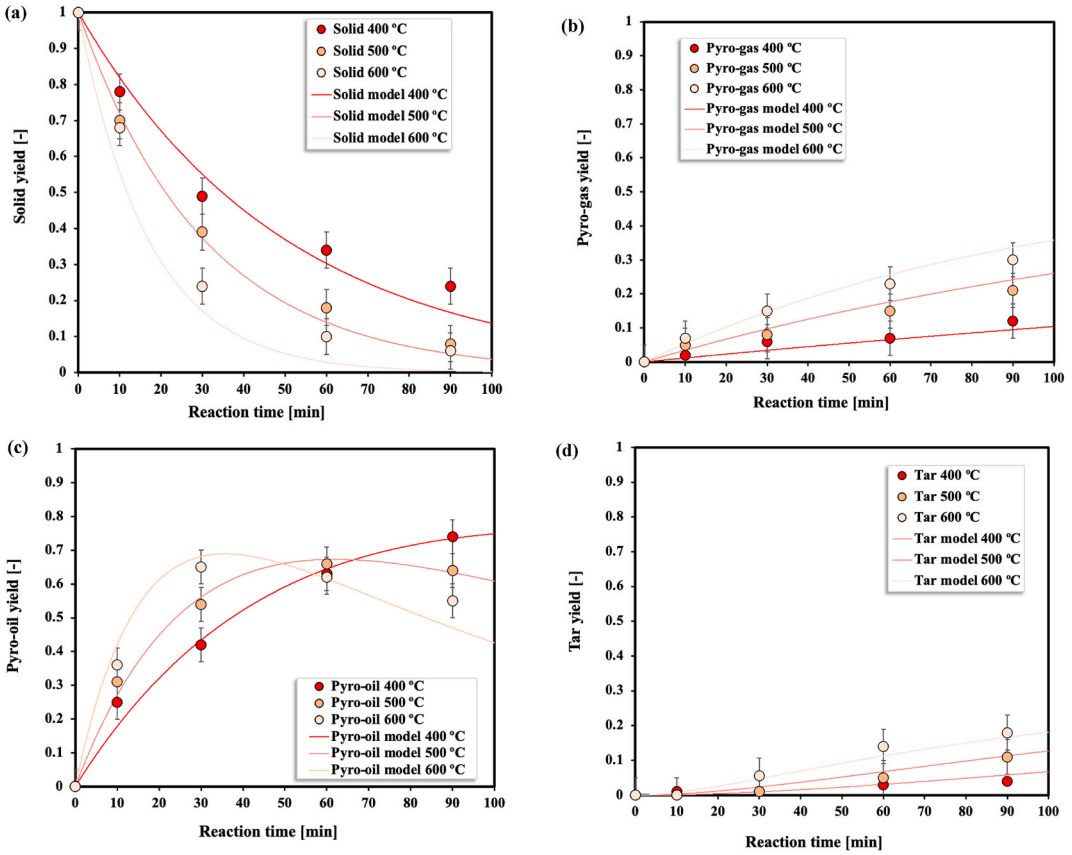

Fig. 6. Effect of temperature and residence time on (a) solid yield, (b) pyro-gas yield, (c) pyro-oil yield, (d) tar yield.

Table 2
The reaction rate constant, activation energy, and order reaction for *Padina* sp. conversion via slow-pyrolysis.

Reaction symbol	Reaction route	The reaction rate constant (k) $[(\text{mol-C/L})^{1-x}\ s^{-1}$			*Ea* [kJ/mol]	Order of reaction, x
		400	500	600		
k_1, x_{sfpg}	solid feedstock ⟶ pyro-gas	0.0199	0.0328	0.0588	26.24	1 (assumed)
k_2, x_{sfpo}	solid feedstock ⟶ pyro-oil	0.0012	0.0036	0.0056	38.12	1 (assumed)
k_3, x_{popg}	pyro-oil ⟶ pyro-gas	0.0010	0.0028	0.0048	38.63	1 (assumed)
k_4, x_{potr}	pyro-oil ⟶ tar	0.0013	0.0023	0.0033	64.42	1.25

energies between 26.24 and 64.42 kJ/mol were obtained for *Padina* sp. pyrolysis.

Interestingly, the activation energy (*Ea*) needed to transform pyro-oil into tar is roughly double (64.42 kJ/mol) that needed to convert a solid into pyro-gas, a solid into pyro-gas or a liquid into pyro-gas, all of which are in the range of 26.24, 38.12, and 38.63 kJ/mol, respectively. This finding is in accordance with the previous study that reported *Ea* required to produce char/tar via polymerization of intermediate products was significantly greater than *Ea* necessary for direct solid conversion of OM in DSS [29]. This could be explained by the fact that the energy required to convert pyro-oil into tar products is more significant than that required to convert solids into pyro-gas or pyro-oil.

The rate constant of tar formation was increased, followed by increased pyrolysis temperature (0.0013 s^{-1} at 400 °C; 0.0023 s^{-1} at 500 °C; and 0.0033 s^{-1} at 600 °C), respectively. Fig. 7 depicts a comparison of this value with findings from earlier investigations. Compared this value to those from Palla et al. [30], Jamilatun et al. [31], and Sasaki et al. [32], it looks to be on the lower range. It is important to note that the difference in reactor diameter impacts the reaction processes occurring during the process. Notably that our reactor diameter (4.85 cm) was more significant than those of Sasaki et al. (0.6 cm), Palla et al. (2.5 cm), and Jamilatun et al. (4.0 cm). The stainless steel construction may have a negative catalytic effect. We intend to investigate this catalytic effect of the reactor wall in the near future.

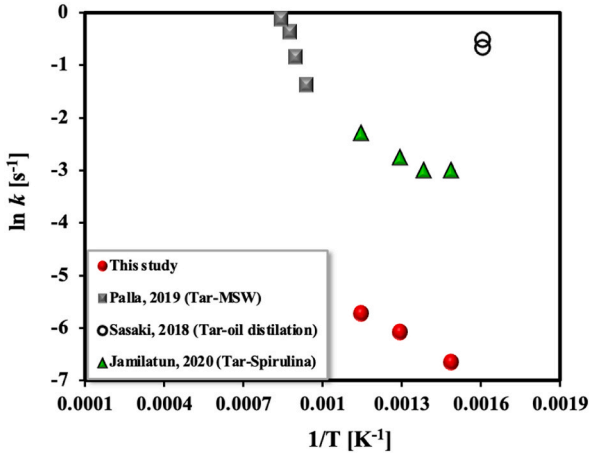

Fig. 7. Comparison between reaction rate constant for tar formation obtained in this study and reaction rate constant from the previous study.

4. Conclusion

Brown macroalgae *Padina* sp. was subjected to pyrolysis and kinetic study in a temperature range of 400, 500, and 600 °C. Several characteristic tests, i.e., element analysis, product distribution, GC-MS analyses as well as tar formation rate constant, were conducted in the study. The maximum pyro-oil yield (67 wt%) was achieved at 500 °C within 60 min. Meanwhile, the highest solid yield (78 wt%) was obtained at 400 °C within 10 min. The main compounds obtained in pyro-oil are N-aromatic (3.6–19.62%), carboxylic acid (6.3–28.0%), aliphatic hydrocarbon (8.32–17.12%), phenols (2.7–3.5%) with the trace amount of ketone, alkanes, and amines/amides. As indicated, pyrolysis at low temperatures did not favor preserving polar functional groups, whereas high temperatures did. The increased tar output was primarily due to forming of many aliphatic and aromatic compounds at the pyrolysis temperature of 500 to 600 °C. To properly duplicate the results of the experiments, a reaction model was developed, and the reaction rate constants were successfully determined. The rate constant of tar formation was determined in a range of 0.0013–0.0033 s^{-1}. A reaction order of 1.25 was determined for the tar formation.

Declarations

Author contribution statement

Apip Amrullah: Conceived and designed the experiments; Performed the experiments; Analyzed and interpreted the data; Wrote the paper.

Obie Farobie: Contributed reagents, materials, analysis tools or data; Wrote the paper.

Data availability statement

Data included in article/supplementary material/referenced in article.

Additional information

No additional information is available for this paper.

Funding

This study was supported by The Directorate General of Higher Education, Research and Technology, Ministry of Education, Culture, Research and Technology, Republic of Indonesia for the funding of this project, Grant Number 113/E5/PG.02.00.PT/2022.

Declaration of competing interest

The authors declare that they have no known competing financial interests or personal relationships that could have appeared to influence the work reported in this paper.

Acknowledgments

The authors gratefully acknowledge The Directorate General of Higher Education, Research and Technology, Ministry of Education, Culture, Research and Technology, Republic of Indonesia, for funding this project. A. Amrullah is also grateful to the Univerisity of Lambung Mangkurat, South Kalimantan, Indonesia.

References

[1] B. Steffen, A. Patt, A historical turning point? Early evidence on how the Russia-Ukraine war changes public support for clean energy policies, Energy Res. Social Sci. 91 (2022), 102758, https://doi.org/10.1016/j.erss.2022.102758.
[2] I. Ko, N. Dolšak, A. Prakash, Have renewable energy leaders announced aggressive emission reduction goals? Examining variations in the stringency of country-level net-zero emission pledges, PLOS Climate 1 (2022), e0000094, https://doi.org/10.1371/journal.pclm.0000094.
[3] O. Farobie, Y. Matsumura, N. Syaftika, A. Amrullah, E. Hartulistiyoso, A. Bayu, N.R. Moheimani, S. Karnjanakom, G. Saefurahman, Recent advancement on hydrogen production from macroalgae via supercritical water gasification, Bioresour. Tech. Rep. 16 (2021), 100844, https://doi.org/10.1016/j.biteb.2021.100844.
[4] J.M. Greene, J. Gulden, G. Wood, M. Huesemann, J.C. Quinn, Techno-economic analysis and global warming potential of a novel offshore macroalgae biorefinery, Algal Res. 51 (2020), https://doi.org/10.1016/j.algal.2020.102032.
[5] J.J. Milledge, B. Smith, P.W. Dyer, P. Harvey, Macroalgae-derived biofuel: a review of methods of energy extraction from seaweed biomass, Energies 7 (2014) 7194–7222, https://doi.org/10.3390/en7117194.
[6] M. Hutomo, M.K. Moosa, Indonesian marine and coastal biodiversity: present status, Indian J. Mar. Sci. 34 (2005) 88–97.
[7] O. Farobie, N. Syaftika, E. Hartulistiyoso, A. Amrullah, A. Bayu, N.R. Moheimani, Y. Matsumura, S. Karnjanakom, The potential of sustainable biogas production from macroalgae in Indonesia, IOP Conf. Ser. Earth Environ. Sci. 1038 (2022), https://doi.org/10.1088/1755-1315/1038/1/012020.
[8] R. Pangestuti, M. Haq, P. Rahmadi, B.S. Chun, Nutritional value and biofunctionalities of two edible green seaweeds (Ulva lactuca and caulerpa racemosa) from Indonesia by subcritical water hydrolysis, Mar. Drugs 19 (2021), https://doi.org/10.3390/md19100578.
[9] M.A. Rimmer, S. Larson, I. Lapong, A.H. Purnomo, P.R. Pong-masak, L. Swanepoel, N.A. Paul, Seaweed aquaculture in Indonesia contributes to social and economic aspects of livelihoods and community wellbeing, Sustainability 13 (2021) 1–22, https://doi.org/10.3390/su131910946.
[10] O. Farobie, E. Hartulistiyoso, Palm oil biodiesel as a renewable energy resource in Indonesia: current status and challenges, Bioenergy Res. 15 (2022) 93–111, https://doi.org/10.1007/s12155-021-10344-7.
[11] M.I. Jahirul, M.G. Rasul, A.A. Chowdhury, N. Ashwath, Biofuels production through biomass pyrolysis- A technological review, Energies 5 (2012) 4952–5001, https://doi.org/10.3390/en5124952.
[12] R. Dolah, R. Karnik, H. Hamdan, A comprehensive review on biofuels from oil palm empty bunch (Efb): current status, potential, barriers and way forward, Sustainability (2021) 13, https://doi.org/10.3390/su131810210.
[13] Z. Huang, J. Zhang, M. Pan, Y. Hao, R. Hu, W. Xiao, G. Li, T. Lyu, Valorisation of microalgae residues after lipid extraction: pyrolysis characteristics for biofuel production, Biochem. Eng. J. 179 (2022), 108330, https://doi.org/10.1016/j.bej.2021.108330.
[14] G. Li, X. Bai, S. Huo, Z. Huang, Fast pyrolysis of LERDADEs for renewable biofuels, IET Renew. Power Gener. 14 (2020) 959–967, https://doi.org/10.1049/iet-rpg.2019.0852.
[15] A. Amrullah, O. Farobie, R. Widyanto, Pyrolysis of purun tikus (Eleocharis dulcis): product distributions and reaction kinetics, Bioresour. Tech. Rep. 13 (2021), 100642, https://doi.org/10.1016/j.biteb.2021.100642.
[16] C. Yang, R. Li, B. Zhang, Q. Qiu, B. Wang, H. Yang, Y. Ding, C. Wang, Pyrolysis of microalgae: a critical review, Fuel Process. Technol. 186 (2019) 53–72, https://doi.org/10.1016/j.fuproc.2018.12.012.
[17] R. Verma, S.K. Verma, V. Verma, S. Verma, Y. Vaishnav, V. Jena, A. Kumar, K.P. Rakesh, Catalytic pyrolysis of ulva lactuca macroalgae: effects of mono and bimetallic catalysts and reaction parameters on bio-oil up-gradation, Bioresour. Technol. 324 (2021), 124594, https://doi.org/10.1016/j.biortech.2020.124594.
[18] H.V. Ly, S.S. Kim, H.C. Woo, J.H. Choi, D.J. Suh, J. Kim, Fast pyrolysis of macroalga Saccharina japonica in a bubbling fluidized-bed reactor for bio-oil production, Energy 93 (2015) 1436–1446, https://doi.org/10.1016/j.energy.2015.10.011.
[19] O. Farobie, A. Amrullah, A. Bayu, N. Syaftika, L.A. Anis, E. Hartulistiyoso, In-depth study of bio-oil and biochar production from macroalgae Sargassum sp. via slow pyrolysis, RSC Adv. 12 (2022) 9567–9578, https://doi.org/10.1039/d2ra00702a.
[20] M.S.J. Sofiana, Y.A. Nurrahman, Warsidah, S. Minsas, A. Yuliono, I. Safitri, S. Helena, Risko, community structure of macroalgae in lemukutan island, Jurnal Ilmu Kelautan 8 (2022) 1–8.
[21] G. Scheffknecht, A. Gredinger, R. Sp, Biomass and Bioenergy Comparison Measurements of Tar Content in Gasi Fi Cation Systems between an Online Method and the Tar Protocol, 2018, p. 111, https://doi.org/10.1016/j.biombioe.2017.01.026.
[22] F. Nie, T. Meng, Q. Zhang, Pyrolysis of low-rank coal: from research to practice, Pyrolysis (2017), https://doi.org/10.5772/67498.
[23] N. Agnihotri, M.K. Mondal, Comparison of non-catalytic and in-situ catalytic pyrolysis of Melia azedarach sawdust, J. Anal. Appl. Pyrol. 172 (2023), 106006, https://doi.org/10.1016/j.jaap.2023.106006.
[24] J.H. Choi, S.S. Kim, D.J. Suh, E.J. Jang, K. Il Min, H.C. Woo, Characterization of the bio-oil and bio-char produced by fixed bed pyrolysis of the brown alga Saccharina japonica, Kor. J. Chem. Eng. 33 (2016) 2691–2698, https://doi.org/10.1007/s11814-016-0131-5.
[25] R.W.R. Zwart, B.J. Vreugdenhil, Tar Formation in Pyrolysis and Gasification, 2009, p. 37.
[26] M.S. Jesus, A. Napoli, P.F. Trugilho, Á.A. Abreu Júnior, C.L.M. Martinez, T.P. Freitas, Energy and mass balance in the pyrolysis process of eucalyptus wood, Cerne 24 (2018) 288–294, https://doi.org/10.1590/01047760201824032561.
[27] A. Aboulkas, H. Hammani, M. El Achaby, E. Bilal, A. Barakat, K. El harfi, Valorization of algal waste via pyrolysis in a fixed-bed reactor: production and characterization of bio-oil and bio-char, Bioresour. Technol. 243 (2017) 400–408, https://doi.org/10.1016/j.biortech.2017.06.098.
[28] J.Y. Kim, J. Moon, J.H. Lee, X. Jin, J.W. Choi, Conversion of phenol intermediates into aromatic hydrocarbons over various zeolites during lignin pyrolysis, Fuel 279 (2020), 118484, https://doi.org/10.1016/j.fuel.2020.118484.
[29] C. Wang, W. Zhu, H. Zhang, C. Chen, X. Fan, Y. Su, Char and tar formation during hydrothermal gasification of dewatered sewage sludge in subcritical and supercritical water: influence of reaction parameters and lumped reaction kinetics, Waste Manag. 100 (2019) 57–65, https://doi.org/10.1016/j.wasman.2019.09.011.
[30] G. Palla, A. Antonin, P. Jean, M. Lavoie, Utilization of MSW-derived char for catalytic reforming of tars and light hydrocarbons in the primary syngas produced during wood chips and MSW-RDF air gasification, Waste Biomass Valoriz. 10 (2019) 1203–1222, https://doi.org/10.1007/s12649-017-0138-0.
[31] S. Jamilatun, E. Sulistiawati, S. Amelia, A. Budiman, Non-catalytic and catalytic pyrolysis of spirulina platensis residue (SPR) in fixed-bed reactors : characteristic and kinetic study with primary and secondary, Tar. Crack. Mod. 10 (2020).
[32] M. Sasaki, M. Goto, Kinetic Study for Liquefaction of Tar in Sub- and Supercritical Water, vol. 93, 2008, pp. 1194–1204, https://doi.org/10.1016/j.polymdegradstab.2008.02.006.